

# NAVAL POSTGRADUATE SCHOOL MONTEREY, CALIFORNIA



## THESIS

### 3-D FINITE ELEMENT METHOD FOR MICROMECHANICAL ANALYSIS IN FIBROUS COMPOSITE MATERIAL

by

Chun-Chung Cheng

June, 1995

Thesis Advisors:

Young W. Kwon  
Robert Mitchel Keolian

Approved for public release; distribution is unlimited.

DTIC QUALITY INSPECTED 3

19960111 040

REPORT DOCUMENTATION PAGE			Form Approved OMB No. 0704-0188	
Public reporting burden for this collection of information is estimated to average 1 hour per response, including the time for reviewing instruction, searching existing data sources, gathering and maintaining the data needed, and completing and reviewing the collection of information. Send comments regarding this burden estimate or any other aspect of this collection of information, including suggestions for reducing this burden, to Washington Headquarters Services, Directorate for Information Operations and Reports, 1215 Jefferson Davis Highway, Suite 1204, Arlington, VA 22202-4302, and to the Office of Management and Budget, Paperwork Reduction Project (0704-0188) Washington DC 20503.				
1. AGENCY USE ONLY (Leave blank)		2. REPORT DATE June 1995		3. REPORT TYPE AND DATES COVERED Master's Thesis
4. TITLE AND SUBTITLE 3-D FINITE ELEMENT METHOD FOR MICROMECHANICAL ANALYSIS IN FIBROUS COMPOSITE MATERIAL			5. FUNDING NUMBERS	
6. AUTHOR(S) Chun-Chung Cheng				
7. PERFORMING ORGANIZATION NAME(S) AND ADDRESS(ES) Naval Postgraduate School Monterey CA 93943-5000			8. PERFORMING ORGANIZATION REPORT NUMBER	
9. SPONSORING/MONITORING AGENCY NAME(S) AND ADDRESS(ES)			10. SPONSORING/MONITORING AGENCY REPORT NUMBER	
11. SUPPLEMENTARY NOTES The views expressed in this thesis are those of the author and do not reflect the official policy or position of the Department of Defense or the U.S. Government.				
12a. DISTRIBUTION/AVAILABILITY STATEMENT Approved for public release; distribution is unlimited.			12b. DISTRIBUTION CODE	
13. ABSTRACT (maximum 200 words)  The objective of this thesis was to study whether simplified three dimensional finite element models could be used as a micromechanical model for analysis of stresses at the fiber and matrix level while providing smeared composite properties for the global structural analysis. The mathematical model was programmed using the MATLAB engineering software. For considering interface cracks between the fiber and matrix, springs were modeled in the connecting nodes between the fiber and matrix on each of the three degrees of freedom. When results were compared with experimental data, findings proved that the simplified three dimensional finite element models could simulate the material property of the graphite/epoxy composite very efficiently.				
14. SUBJECT TERMS composites, composite material, fibrous composite, finite element, finite element method, micromechanical analysis, 3-D FEM			15. NUMBER OF PAGES 60	
			16. PRICE CODE	
17. SECURITY CLASSIFICATION OF REPORT Unclassified	18. SECURITY CLASSIFICATION OF THIS PAGE Unclassified	19. SECURITY CLASSIFICATION OF ABSTRACT Unclassified	20. LIMITATION OF ABSTRACT UL	



Approved for public release; distribution is unlimited.

3-D FINITE ELEMENT METHOD FOR MICROMECHANICAL  
ANALYSIS IN FIBROUS COMPOSITE MATERIAL

Chun-Chung Cheng  
Major, Republic of China Army  
B.S., Chung-Cheng Institute of Technology, 1972

Submitted in partial fulfillment  
of the requirements for the degree of

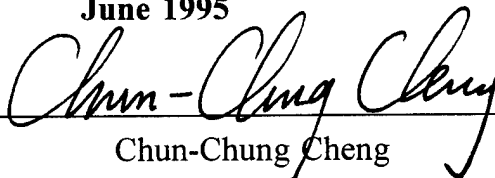
**MASTER OF SCIENCE IN APPLIED PHYSICS**

from the


**NAVAL POSTGRADUATE SCHOOL**

**June 1995**

Author:

  
Chun-Chung Cheng

Approved by:

  
Young W. Kwon, Thesis Advisor



Robert Mitchel Keolian, Second Reader



William Colson, Chairman  
Department of Physics



## ABSTRACT

The objective of this thesis was to study whether simplified three dimensional finite element models could be used as a micromechanical model for analysis of stresses at the fiber and matrix level while providing smeared composite properties for the global structural analysis. The mathematical model was programmed using the MATLAB engineering software. For considering interface cracks between the fiber and matrix, springs were modeled in the connecting nodes between the fiber and matrix on each of the three degrees of freedom. When results were compared with experimental data, findings proved that the simplified three dimensional finite element models could simulate the material property of the graphite/epoxy composite very efficiently.

Accession For	
NTIS CRA&I	<input checked="" type="checkbox"/>
DTIC TAB	<input checked="" type="checkbox"/>
Unannounced	<input type="checkbox"/>
Justification _____	
By _____	
Distribution /	
Availability Codes	
Dist	Avail and/or Special
A-1	



## TABLE OF CONTENTS

I. INTRODUCTION .....	1
II. MICROMECHANICAL MODELS .....	5
A. ANALYTICAL MICROMECHANICAL MODELS .....	5
B. FEM MICROMECHANICAL MODEL .....	11
1. Three Dimensional Finite Element Method .....	11
2. Interface Crack .....	21
C. MATLAB COMPUTER PROGRAM DEVELOPMENT .....	22
III. RESULTS AND DISCUSSION .....	23
IV. CONCLUSIONS AND RECOMMENDATION .....	41
REFERENCE LIST .....	43
APPENDIX A .....	45
APPENDIX B .....	47
APPENDIX C .....	49
INITIAL DISTRIBUTION LIST .....	51



## I. INTRODUCTION

Fibrous composite material is useful for structural application because of its beneficial material properties such as high ratios of stiffness-to-weight and strength-to-weight. In fibrous composite, fibers are embedded in a matrix material. The matrix, besides holding the fibers together, has an important function of transferring the applied load among the fibers.

In order to analyze the fibrous composite structure, it is necessary to obtain material properties for the composite. The material properties can be obtained from experiments. However, some material properties are not easy to measure directly from the physical test. In addition, if there is a different fiber volume fraction, the composite material properties also vary even if the same fiber and matrix materials constitute the composite. As a result, it is useful to predict the material properties of a composite, given the component properties and their geometric arrangement.

The objective of this study is to develop a micromechanical model to determine the composite properties when the fiber and matrix materials are known as well as the fiber volume fraction. There have been many studies for this purpose so far. However, most of the studies were two-dimensional models so that they provided limited information. A small number of three-dimensional models were proposed [Ref. 1-3]. These three-dimensional micromechanics

models assumed perfect bonding at the fiber/matrix interface. In order to model a more general case including partial interface crack, a simplified three-dimensional finite element model is developed in this study and the results are compared to available experimental results.

Figure 1 shows the micromechanical modeling process. The micromechanics model considers a fiber surrounded by a matrix material. In the following chapters, both analytical and finite element micromechanical models are presented, as well as their results for perfect interfacial bonding and partial interfacial cracks. Conclusions and recommendation follow.

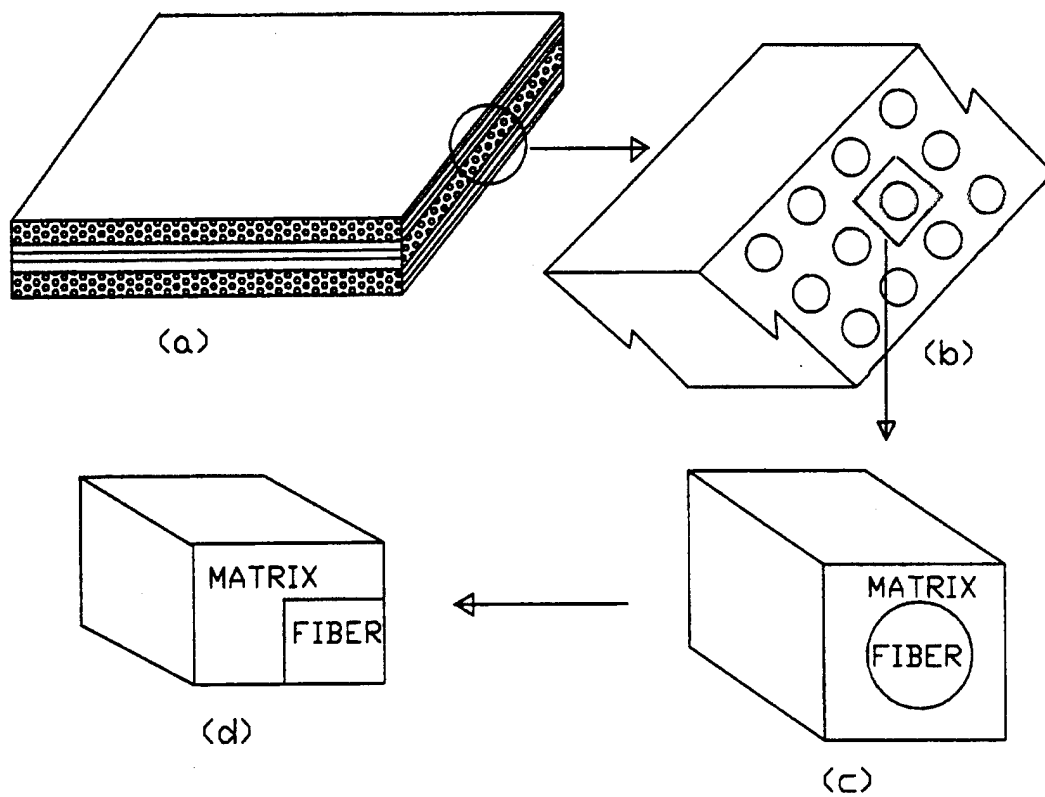


**Figure 1** (a) to (d) shows macromechanical analysis of a laminate composites and micromechanic analysis of a thin unidirection lamina.



## II. MICROMECHANICAL MODELS

### A. ANALYTICAL MICROMECHANICAL MODEL

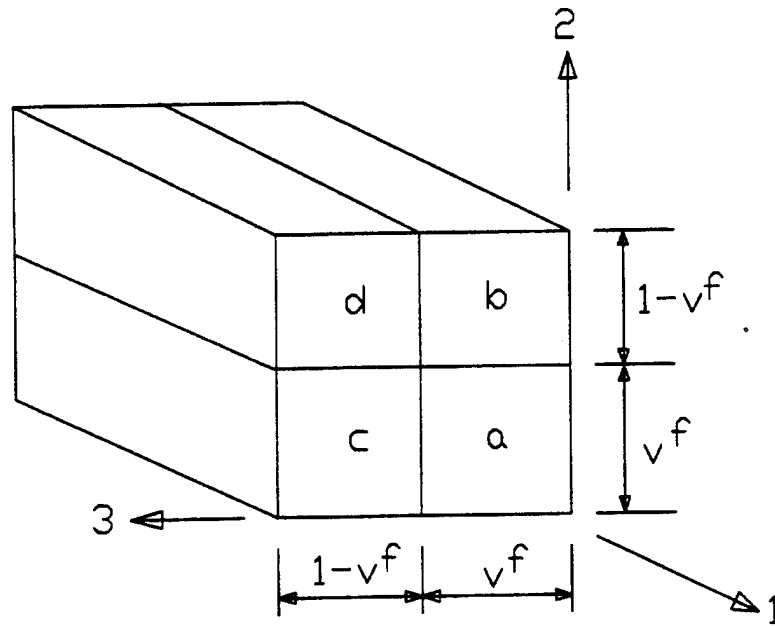
Kwon's micro-mechanics model considers a unit cell consisting of the fiber and surrounding matrix material. The fiber is assumed to have a square cross-section. Based on symmetry consideration, a quarter of the unit cell is divided into four subcells. The size of subcell depends on the fiber volume fraction, as shown in Figure 2. The stress continuity at the subcell interfaces is expressed as

$$\begin{aligned}\sigma_{22}^a &= \sigma_{22}^b, & \sigma_{22}^c &= \sigma_{22}^d, & \sigma_{33}^a &= \sigma_{33}^c, & \sigma_{33}^b &= \sigma_{33}^d \\ \sigma_{12}^a &= \sigma_{12}^b, & \sigma_{12}^c &= \sigma_{12}^d, & \sigma_{13}^a &= \sigma_{13}^c, & \sigma_{13}^b &= \sigma_{13}^d \\ \sigma_{23}^a &= \sigma_{23}^b = \sigma_{23}^c = \sigma_{23}^d\end{aligned}\tag{2.1}$$

and the strain compatibility is assumed as

$$\begin{aligned}\epsilon_{11}^a &= \epsilon_{11}^b = \epsilon_{11}^c = \epsilon_{11}^d \\ \epsilon_{22}^a + \epsilon_{22}^b &= \epsilon_{22}^c + \epsilon_{22}^d, & \epsilon_{33}^a + \epsilon_{33}^c &= \epsilon_{33}^b + \epsilon_{33}^d \\ \epsilon_{12}^a + \epsilon_{12}^b &= \epsilon_{12}^c + \epsilon_{12}^d, & \epsilon_{13}^a + \epsilon_{13}^c &= \epsilon_{13}^b + \epsilon_{13}^d\end{aligned}\tag{2.2}$$

The constitutive relation for each subcell is expressed by the generalized Hooke's law of Equation (2.3)



a- FIBER SUBCELL  
b, c and d - MATRIX SUBCELLS

**Figure 2** A unit cell made of subcell

$$\sigma_{ij}^{\alpha} = E_{ijkl}^{\alpha} \epsilon_{kl}^{\alpha} \quad (2.3)$$

$$i, j, k, l = 1, 2, 3 \quad \text{and} \quad \alpha = a, b, c, d$$

The size of each subcell depends on the fiber volume fraction. Kwon expressed the composite stresses and strains as a function of the subcell stresses, the subcell strains, and the fiber volume fraction as shown in Equation (2.4)

$$\begin{aligned} \bar{\sigma}_{ij} &= V_f \sigma_{ij}^a + \sqrt{V_f} (1 - \sqrt{V_f}) \sigma_{ij}^b + \sqrt{V_f} (1 - \sqrt{V_f}) \sigma_{ij}^c + (1 - \sqrt{V_f})^2 \sigma_{ij}^d \\ \bar{\epsilon}_{ij} &= V_f \epsilon_{ij}^a + \sqrt{V_f} (1 - \sqrt{V_f}) \epsilon_{ij}^b + \sqrt{V_f} (1 - \sqrt{V_f}) \epsilon_{ij}^c + (1 - \sqrt{V_f})^2 \epsilon_{ij}^d \end{aligned} \quad (2.4)$$

$$i, j = 1, 2, 3$$

where  $\bar{\sigma}_{ij}$  and  $\bar{\epsilon}_{ij}$  are composite stresses and strains,  $\sigma_{ij}^{\alpha}$  and  $\epsilon_{ij}^{\alpha}$  are stresses and strains of a subcell ( $\alpha = a, b, c$  or  $d$ ),  $V_f$  is the fiber volume fraction, and subcell 'a' represents a fiber and the rest of the subcells are matrix. The composite stresses or strains are determined by the volume average of the stresses and strains of the subcells.

Instead of the second and third expressions in Equation (2.2), we may assume the following deformation compatibility

$$\begin{aligned} \sqrt{V_f} \epsilon_{22}^a + (1 - \sqrt{V_f}) \epsilon_{22}^b &= \sqrt{V_f} \epsilon_{22}^c + (1 - \sqrt{V_f}) \epsilon_{22}^d \\ \sqrt{V_f} \epsilon_{33}^a + (1 - \sqrt{V_f}) \epsilon_{33}^c &= \sqrt{V_f} \epsilon_{33}^b + (1 - \sqrt{V_f}) \epsilon_{33}^d \end{aligned} \quad (2.5)$$

This is the primary difference from Kwon's analytical model.

Some algebraic operations are conducted for Equation (2.1) through (2.5) to relate the subcell strains to cell strains (composite strains) as given in Equation (2.6).

$$[A]\{\epsilon_{ij}^{\alpha}\} = \{\bar{\epsilon}_{ij}\} \quad i, j = 1, 2, 3 \quad (2.6)$$

Inverting the coefficient matrix  $[A]$ , Equation (2.6) can be also written as

$$\{\epsilon_{ij}^{\alpha}\} = [A]^{-1}\{\bar{\epsilon}_{ij}\} \quad (2.7)$$

Use of Equation (2.3), the first Equation of (2.4) and Equation (2.7) results in relation between composite stresses and strains, That is

$$\{\bar{\sigma}_{ij}\} = [C]\{\bar{\epsilon}_{ij}\} \quad (2.8)$$

where matrix  $[C]$  is the smeared material property matrix for the composite.

Assuming orthotropic materials for the fiber and matrix, normal stress and strain components are uncoupled from shear stress and strain components. In this case, the equations relating subcell strains to cell strains for the normal strains are given in Appendix A.

The comparison between analytical and experimental results is shown in Figure 3, for the transverse elastic modulus of a graphite/epoxy composite whose material properties are shown in Table 1. The modified analytical solution agrees slightly better with the experimental data than the original analytical solution in



Ref. [1]. However, other properties such as longitudinal elastic modulus, shear modulus, and Poisson's ratio were not different between the two analytical solutions which agreed well with the experimental data.

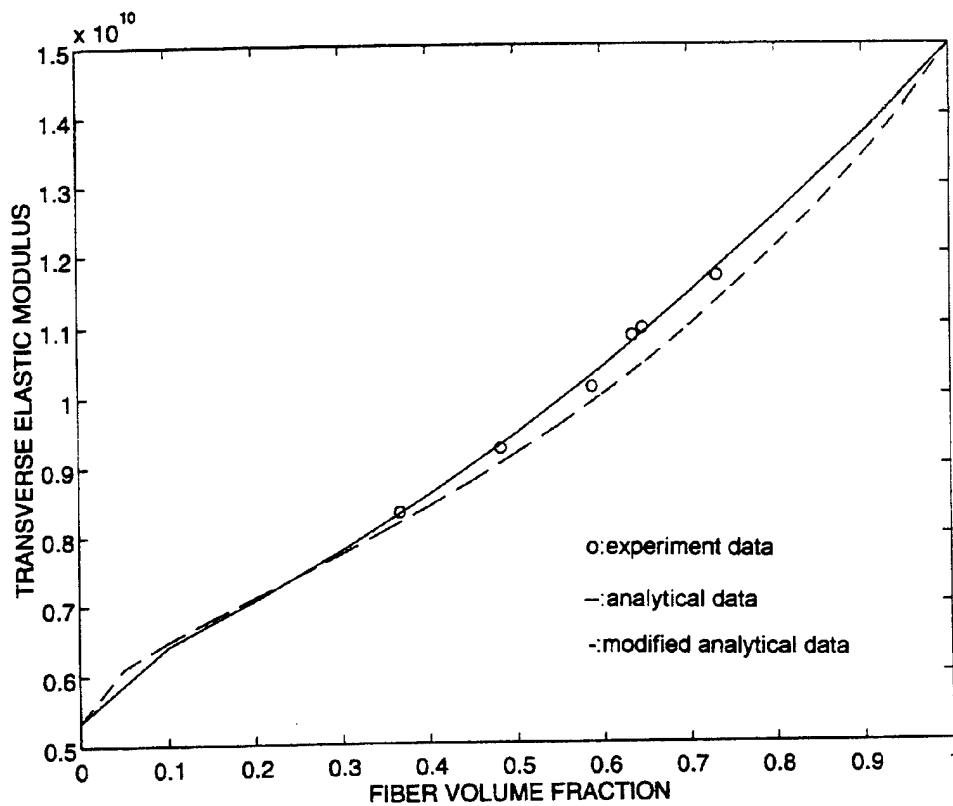


**Figure 3** Transverse elastic modulus of a graphite/epoxy composite

Table 1 Characteristic Of Matrix And Fibers In The Graphite/Epoxy Composites

Properties	Graphite Fiber	Epoxy Matrix
Longitudinal elastic Modulus (Gpa)	232	5.35
Transverse ealstic Modulus (Gpa)	15	5.35
Longitudinal Poisson's Ratio	0.275	0.354
Transverse Poisson's Ratio	0.49	0.354
Inplane Shear Modulus (Gpa)	24	NA

\* Graphite fiber is transversely isotropic material  
Epoxy matrix is isotropic material

## **B. FEM MICROMECHANICAL MODEL**

The finite element method [Ref. 4, 5] is a numerical technique which gives an approximate solution to differential equations that model physical and engineering problems. The finite element method requires a problem, which is defined in a geometrical space (or domain), to be subdivided into a finite number of smaller regions (mesh). Over each finite element, the unknown variables are approximated by using nodal variables; these functions can be linear or higher order polynomial expressions that depend on the node numbers and their locations used to define the finite element shape. The governing differential equations are transformed into a matrix expression over each finite element and the matrix expressions are summed ("assembled") over the entire problem domain. As a result, a set of linear equations is obtained in terms of the unknown nodal variables. In this section, the three dimensional finite element method is introduced followed by a discussion of the programming procedure :

### **1. Three Dimensional Finite Element Method**

The Galerkin form of the weighted residual procedure is adopted to formulate the finite element method. The idea of the weighted residual method is that we multiply the residual by a weighting function and enforce the integral of the weighted expression to vanish. The finite element formulation for three-dimensional elasticity can be shown below :

The equilibrium equations are

$$\begin{aligned}
\frac{\partial \sigma_x}{\partial x} + \frac{\partial \tau_{xy}}{\partial y} + \frac{\partial \tau_{xz}}{\partial z} &= 0 \\
\frac{\partial \tau_{yx}}{\partial x} + \frac{\partial \sigma_y}{\partial y} + \frac{\partial \tau_{yz}}{\partial z} &= 0 \\
\frac{\partial \tau_{zx}}{\partial x} + \frac{\partial \tau_{zy}}{\partial y} + \frac{\partial \sigma_z}{\partial z} &= 0
\end{aligned} \tag{2.9}$$

where the shear stresses satisfy the following relation

$$\begin{aligned}
\tau_{xy} &= \tau_{yx} \\
\tau_{xz} &= \tau_{zx} \\
\tau_{yz} &= \tau_{zy}
\end{aligned} \tag{2.10}$$

due to symmetric stress tensor.

The first step in the FEM is to convert the partial differential equations into an integral expression by applying the method of weighted residual to the three dimensional stress equilibrium equations (2.9). Each equation is multiplied by a weight function  $W_i$  ( $i=1,2,3$ ), which is continuous over the physical domain of the problem. The resulting weighted residual equations are

$$\begin{aligned}
I &= \iiint_V \left( \frac{\partial \sigma_x}{\partial x} + \frac{\partial \tau_{xy}}{\partial y} + \frac{\partial \tau_{xz}}{\partial z} \right) W_1 dV = 0 \\
I &= \iiint_V \left( \frac{\partial \tau_{yx}}{\partial x} + \frac{\partial \sigma_y}{\partial y} + \frac{\partial \tau_{yz}}{\partial z} \right) W_2 dV = 0 \\
I &= \iiint_V \left( \frac{\partial \tau_{zx}}{\partial x} + \frac{\partial \tau_{zy}}{\partial y} + \frac{\partial \sigma_z}{\partial z} \right) W_3 dV = 0
\end{aligned} \tag{2.11}$$

Applying integration by parts and combining the three expressions yields

$$\iiint_V \left\{ \begin{array}{l} \sigma_x \frac{\partial W_1}{\partial x} + \tau_{xy} \frac{\partial W_1}{\partial y} + \tau_{xz} \frac{\partial W_1}{\partial z} \\ \tau_{xy} \frac{\partial W_2}{\partial x} + \sigma_y \frac{\partial W_2}{\partial y} + \tau_{yz} \frac{\partial W_2}{\partial z} \\ \tau_{xz} \frac{\partial W_3}{\partial x} + \tau_{yz} \frac{\partial W_3}{\partial y} + \sigma_z \frac{\partial W_3}{\partial z} \end{array} \right\} dV = \iint_S \left\{ \begin{array}{l} \phi_x n_x \\ \phi_y n_y \\ \phi_z n_z \end{array} \right\} ds \quad (2.12)$$

where

$$\begin{aligned} \phi_x &= \sigma_x n_x + \tau_{xy} n_y + \tau_{xz} n_z \\ \phi_y &= \tau_{xy} n_x + \sigma_y n_y + \tau_{yz} n_z \\ \phi_z &= \tau_{xz} n_x + \tau_{yz} n_y + \sigma_z n_z \end{aligned} \quad (2.13)$$

are boundary tractions.

Let 'u', 'v', and 'w' represent displacements in the x, y and z direction, respectively. Then, the relationship of strain to displacement, assuming small displacements, can be written as

$$\begin{aligned} \epsilon_x &= \frac{\partial u}{\partial x}, \epsilon_y = \frac{\partial v}{\partial y}, \epsilon_z = \frac{\partial w}{\partial z} \\ \gamma_{xy} &= \left( \frac{\partial u}{\partial y} + \frac{\partial v}{\partial x} \right), \gamma_{yz} = \left( \frac{\partial w}{\partial y} + \frac{\partial v}{\partial z} \right), \gamma_{xz} = \left( \frac{\partial u}{\partial z} + \frac{\partial w}{\partial x} \right) \end{aligned} \quad (2.14)$$

The constitutive relation between stress and strain is

$$\{\sigma\} = [D]\{\epsilon\} \quad (2.15)$$

the material property matrix [D] for a composite material is shown in detail in Appendix B.

Equation (2.12) can be written in matrix form by substituting the strain-displacement Equation (2.14) into the constitutive relation given by (2.15). The resultant expression is shown in Equation (2.16).

$$\iiint_V \left[ \begin{array}{cccccc} \frac{\partial W_1}{\partial x} & 0 & 0 & \frac{\partial W_1}{\partial y} & 0 & \frac{\partial W_1}{\partial z} \\ 0 & \frac{\partial W_2}{\partial y} & 0 & \frac{\partial W_2}{\partial x} & \frac{\partial W_2}{\partial z} & 0 \\ 0 & 0 & \frac{\partial W_3}{\partial z} & 0 & \frac{\partial W_3}{\partial y} & \frac{\partial W_3}{\partial x} \end{array} \right] [D] \left[ \begin{array}{ccc} \frac{\partial}{\partial x} & 0 & 0 \\ 0 & \frac{\partial}{\partial y} & 0 \\ 0 & 0 & \frac{\partial}{\partial z} \\ \frac{\partial}{\partial y} & \frac{\partial}{\partial x} & 0 \\ 0 & \frac{\partial}{\partial z} & \frac{\partial}{\partial y} \\ \frac{\partial}{\partial z} & 0 & \frac{\partial}{\partial x} \end{array} \right] \left\{ \begin{array}{c} u \\ v \\ w \end{array} \right\} dV = \iint_s \left\{ \begin{array}{c} \phi_x n_x \\ \phi_y n_y \\ \phi_z n_z \end{array} \right\} ds \quad (2.16)$$

Eight noded isoparametric rectangular parallelepiped elements are used for the formulation. Each node has three orthogonal displacements, 'u', 'v', and 'w', so that each element has a total of 24 degrees of freedom (dof). In the next step of the FEM, we can define the displacements in terms of polynomial shape functions, named  $H_i$ , as follows

$$u = \sum_{i=1}^8 H_i u_i ; \quad v = \sum_{i=1}^8 H_i v_i ; \quad w = \sum_{i=1}^8 H_i w_i \quad (2.17)$$

The displacement vector of size  $3 \times 1$  can be expressed as the product of a  $3 \times 24$  shape function matrix and a  $24 \times 1$  nodal displacement vector as shown in Appendix C. Taking the first partial derivatives of the shape functions with respect to the coordinates results in the following set of expressions :

$$\begin{aligned}
\frac{\partial u}{\partial x} &= \sum_{i=1}^8 \frac{\partial H_i}{\partial x} u_i & \frac{\partial v}{\partial x} &= \sum_{i=1}^8 \frac{\partial H_i}{\partial x} v_i & \frac{\partial w}{\partial x} &= \sum_{i=1}^8 \frac{\partial H_i}{\partial x} w_i \\
\frac{\partial u}{\partial y} &= \sum_{i=1}^8 \frac{\partial H_i}{\partial y} u_i & \frac{\partial v}{\partial y} &= \sum_{i=1}^8 \frac{\partial H_i}{\partial y} v_i & \frac{\partial w}{\partial y} &= \sum_{i=1}^8 \frac{\partial H_i}{\partial y} w_i \\
\frac{\partial u}{\partial z} &= \sum_{i=1}^8 \frac{\partial H_i}{\partial z} u_i & \frac{\partial v}{\partial z} &= \sum_{i=1}^8 \frac{\partial H_i}{\partial z} v_i & \frac{\partial w}{\partial z} &= \sum_{i=1}^8 \frac{\partial H_i}{\partial z} w_i
\end{aligned} \quad (2.18)$$

The product of the  $6 \times 3$  partial differential matrix of Equation (2.16) and the  $3 \times 24$  shape function matrix are typically combined into one  $6 \times 24$  matrix. This matrix is referred to as the "B" matrix in this development. The "B" matrix can be partitioned into sub-matrices labeled  $B_i$ , where  $i=1$  to 8.

$$[B] = [[B_1][B_2][B_3][B_4][B_5][B_6][B_7][B_8]] \quad (2.19)$$

where

$$[B_i] = \begin{bmatrix} \frac{\partial H_i}{\partial x} & 0 & 0 \\ 0 & \frac{\partial H_i}{\partial y} & 0 \\ 0 & 0 & \frac{\partial H_i}{\partial z} \\ \frac{\partial H_i}{\partial y} & \frac{\partial H_i}{\partial x} & 0 \\ 0 & \frac{\partial H_i}{\partial z} & \frac{\partial H_i}{\partial y} \\ \frac{\partial H_i}{\partial z} & 0 & \frac{\partial H_i}{\partial x} \end{bmatrix} \quad \text{where } i = 1 \text{ to } 8 \quad (2.20)$$

The Galerkin method takes the shape functions as the weighting functions

$$W_1 = W_2 = W_3 = \begin{bmatrix} H_1 \\ H_2 \\ H_3 \\ H_4 \\ H_5 \\ H_6 \\ H_7 \\ H_8 \end{bmatrix} \quad (2.21)$$

Based on the weighting functions shown above, the weighting function matrix in Equation (2.16) can now be written in terms of the shape functions as

$$\begin{bmatrix} \frac{\partial W_1}{\partial x} & 0 & 0 & \frac{\partial W_1}{\partial y} & 0 & \frac{\partial W_1}{\partial z} \\ 0 & \frac{\partial W_2}{\partial y} & 0 & \frac{\partial W_2}{\partial x} & \frac{\partial W_2}{\partial z} & 0 \\ 0 & 0 & \frac{\partial W_3}{\partial z} & 0 & \frac{\partial W_3}{\partial y} & \frac{\partial W_3}{\partial x} \end{bmatrix} = [B]^T \quad (2.22)$$

Therefore, Equation (2.16) can be revised as follows

$$\iiint_v [B]^T [D] [B] dV \{d\} = \iint_s \begin{Bmatrix} \phi_x \{H_i\} \\ \phi_y \{H_i\} \\ \phi_z \{H_i\} \end{Bmatrix} dS \quad (2.23)$$

Actually, the above equation can be expressed in simplified form as

$$[K_e] \{d\} = \{F_e\} \quad (2.24)$$

For a complex geometry, the finite element method employs a mapping between two different coordinate systems. In order to map a regular shaped element in the 'rst' coordinate onto an irregular shaped element in the 'xyz' coordinate, the Jacobian matrix is required. Equation (2.25) shows the Jacobian for mapping between 'rst' system and 'xyz' coordinate system.

$$[J] = \begin{bmatrix} \frac{\partial x}{\partial r} & \frac{\partial y}{\partial r} & \frac{\partial z}{\partial r} \\ \frac{\partial x}{\partial s} & \frac{\partial y}{\partial s} & \frac{\partial z}{\partial s} \\ \frac{\partial x}{\partial t} & \frac{\partial y}{\partial t} & \frac{\partial z}{\partial t} \end{bmatrix} \quad (2.25)$$



In terms of the shape functions and nodal points, the Jacobian is expressed as

$$[J] = \begin{bmatrix} \sum_{i=1}^8 \frac{\partial H_i}{\partial r} x_i & \sum_{i=1}^8 \frac{\partial H_i}{\partial r} y_i & \sum_{i=1}^8 \frac{\partial H_i}{\partial r} z_i \\ \sum_{i=1}^8 \frac{\partial H_i}{\partial s} x_i & \sum_{i=1}^8 \frac{\partial H_i}{\partial s} y_i & \sum_{i=1}^8 \frac{\partial H_i}{\partial s} z_i \\ \sum_{i=1}^8 \frac{\partial H_i}{\partial t} x_i & \sum_{i=1}^8 \frac{\partial H_i}{\partial t} y_i & \sum_{i=1}^8 \frac{\partial H_i}{\partial t} z_i \end{bmatrix} \quad (2.26)$$

Letting  $[J]^{-1} = [\Gamma]$ , the derivatives of shape functions with respect to the 'xyz' system are now expressed in Equation (2.27) with respect to the 'rst' coordinate system.

$$\begin{aligned} \frac{\partial H_i}{\partial x} &= \Gamma_{11} \frac{\partial H_i}{\partial r} + \Gamma_{12} \frac{\partial H_i}{\partial s} + \Gamma_{13} \frac{\partial H_i}{\partial t} \\ \frac{\partial H_i}{\partial y} &= \Gamma_{21} \frac{\partial H_i}{\partial r} + \Gamma_{22} \frac{\partial H_i}{\partial s} + \Gamma_{23} \frac{\partial H_i}{\partial t} \\ \frac{\partial H_i}{\partial z} &= \Gamma_{31} \frac{\partial H_i}{\partial r} + \Gamma_{32} \frac{\partial H_i}{\partial s} + \Gamma_{33} \frac{\partial H_i}{\partial t} \end{aligned} \quad (2.27)$$

The integral in terms of the 'xyz' coordinate can be transformed into the integral in terms of the 'rst' coordinate using the Jacobian matrix.

$$\iiint_v [B]^T [D] [B] dV(x, y, z) \{d\} = \iiint_v [B]^T [D] [B] |J| dV(r, s, t) \{d\} \quad (2.28)$$

where  $|J|$  is the determinant of the Jacobian matrix.

The transformation to the 'rst' coordinate system results in a simplified integral because the element domain is regular in the 'rst' coordinate system. The resultant elements are called isoparametric elements. The term isoparametric refers

to the equality between the degree of the equation for transforming 'xyz' into 'rst' coordinates and the degree of the shape functions for estimating displacement. The shape functions defined in terms of the 'rst' coordinate for the eight-noded brick element are shown in Equation (2.29)

$$\begin{aligned}
 H_1 &= \frac{1}{8}(1+r)(1+s)(1+t) \\
 H_2 &= \frac{1}{8}(1+r)(1-s)(1+t) \\
 H_3 &= \frac{1}{8}(1+r)(1-s)(1-t) \\
 H_4 &= \frac{1}{8}(1+r)(1+s)(1-t) \\
 H_5 &= \frac{1}{8}(1-r)(1+s)(1+t) \\
 H_6 &= \frac{1}{8}(1-r)(1-s)(1+t) \\
 H_7 &= \frac{1}{8}(1-r)(1-s)(1-t) \\
 H_8 &= \frac{1}{8}(1-r)(1+s)(1-t)
 \end{aligned} \tag{2.29}$$

The Gauss quadrature is used for numerical integration. The volume integral is replaced by the triple summation over the number of integration points (NIP) of the integral evaluated at Gauss integration points (r, s, t) and multiplied by weighting factors as shown in Equation (2.30)

$$\iiint_v [B]^T [D] [B] |J| dV(r, s, t) \{d\} = \sum_{i=1}^{NIP} \sum_{j=1}^{NIP} \sum_{k=1}^{NIP} [B]^T [D] [B] |J| W_i W_j W_k \{d\} \tag{2.30}$$

The results of the numerical integration may vary over the elements in the domain of the model. Each of these results can be expressed as a 24×24 matrix which is termed the elemental stiffness matrix [Ke]. The surface traction boundary conditions are from the right hand side of Equation (2.23). The integration of the applied traction over the element surface area results in the

24×1 element force vector  $\{Fe\}$  which represents the lumped forces at the nodal forces in the x, y, z directions. Once the element matrices and vectors are determined, they are assembled into the global system of equations

$$[KK]_{54 \times 54} \{dd\}_{54 \times 1} = \{FF\}_{54 \times 1} \quad (2.31)$$

In order to solve the matrix Equation (2.31), the essential boundary conditions must be applied in advance. In this study, since the cell is symmetric, symmetric boundary conditions are applied to the symmetric planes. In addition, for the displacement boundary control, as shown in Fig 4, a uniform displacement is applied in the micromechanics model. For this case, the elastic modulus can be calculated from

$$E = \frac{\sigma_c}{\varepsilon_c} \quad (2.32)$$

where  $\sigma_c$ , composite average stress, can be calculated from subcell stresses and  $\varepsilon_c$ , composite average strain, calculated from the given displacement condition. For another case, called force boundary control, a uniform traction is applied instead of the displacement. For this condition,  $\sigma_c$  can be obtained from the given force. Then from the displacement change of each node of the subcell, we can calculate the subcell strain. The cell strain  $\varepsilon_c$  is obtained by averaging the subcell strains.

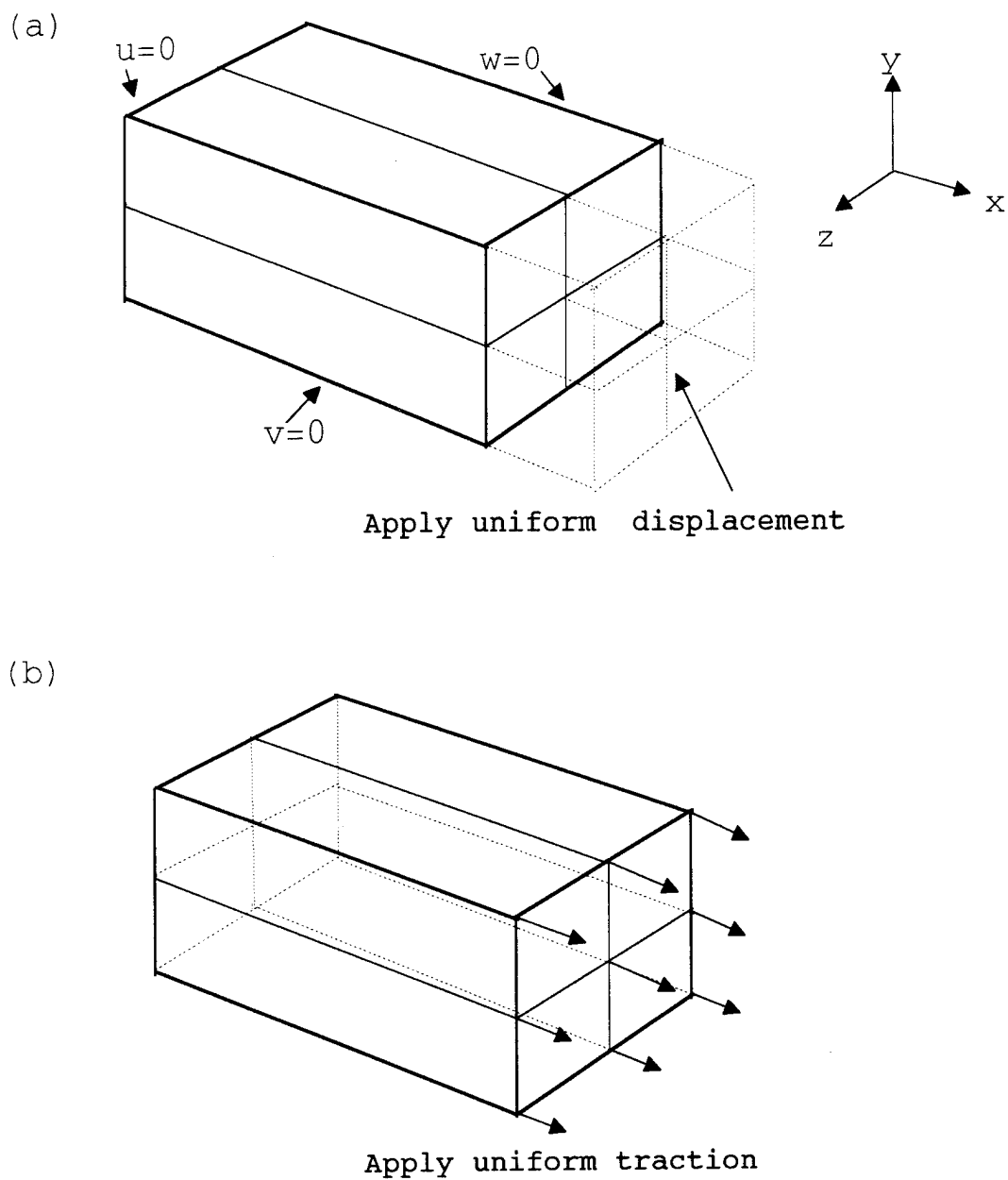


**Figure 4** (a) Displacement boundary control applied on longitudinal or transverse direction  
 (b) Force boundary control applied on longitudinal or transverse direction

## 2. Interface Crack

If there is a partial crack between interface of the fiber and matrix, we assume there is a spring between the connected nodes (between the fiber and matrix elements) in each 'u', 'v', 'w' direction. The spring constants are called  $k_x, k_y, k_z$ . The stiffness matrix for the spring element is

$$\begin{bmatrix} k_x & 0 & 0 & -k_x & 0 & 0 \\ 0 & k_y & 0 & 0 & -k_y & 0 \\ 0 & 0 & k_z & 0 & 0 & -k_z \\ -k_x & 0 & 0 & k_x & 0 & 0 \\ 0 & -k_y & 0 & 0 & k_y & 0 \\ 0 & 0 & -k_z & 0 & 0 & k_z \end{bmatrix} \quad (2.33)$$

We add this stiffness matrix into the global matrix. This matrix equation can calculate the stress and strain of the composite and obtain the composite material property for partial interface crack between the fiber and matrix.

### C. MATLAB COMPUTER PROGRAM DEVELOPMENT

The previously derived finite element formulation was programmed using the MATLAB program to simulate the composite material property for perfect bonding and a partial interface crack between the fiber and matrix. The main procedure of the program is as follows :

1. Input x, y, z coordinates and connectivity to denote the area of the fiber and matrix using NODAL.
2. Input the material properties of fiber and matrix, and calculate the subcell material property matrix [D] using MATER.
3. Using the Gauss-integration technique to calculate the Jacobian matrix, obtain  $[B]^T$  and [B] in the 'rst' coordinate system using GAUSS and JACOBIAN.
4. Compute the local stiffness matrix  $[K_e]$  from  $\sum \sum \sum [B]^T [D] [B] |J| W_i W_j W_k$ .
5. Assemble the local stiffness matrix  $[K_e]$  of each subcell into the system stiffness matrix [KK] using GLOBKF function.
6. Apply boundary conditions to modify the global stiffness matrix using MOD.
7. For the interface crack analysis, the crack stiffness matrix is added to the system stiffness matrix before applying the boundary condition.
8. Post-process to calculate stress and strain in each subcell under either displacement or force boundary control, and calculate the composite stress and strain to obtain the smeared material properties.

### III. RESULTS AND DISCUSSION

Graphite/epoxy is a continuous fibrous composite material. Graphite fibers were considered to be transversely isotropic and the epoxy matrix was considered to be isotropic. The corresponding properties are listed in Table 1. The effective moduli of the composites predicted by three dimensional finite element model were compared to the experimental data [Ref. 6].

For the three dimensional finite element method, elastic and shear moduli in both longitudinal and transverse directions, respectively, are compared as well as the transverse Poisson's ratio. The experimental and computed material properties of the graphite/epoxy composite show good agreement between them. The comparisons are shown in Figure 5 to Figure 9. In general, either the displacement boundary control or the force boundary control produces similar results. However, there is a large difference on longitudinal elastic modulus. In the transverse direction, the predicted results are close each other. Since, in the transverse direction, the acted plane is matrix which is much softer than the fiber, the cell deformation depends on the matrix subcell more than the fiber cell. Otherwise, in the longitudinal direction, the fiber dominates the deformation.

For the interface crack analysis, the spring constants  $k_x$ ,  $k_y$ ,  $k_z$  are assumed five different values,  $10^{11}$ ,  $5 \times 10^{10}$ ,  $2 \times 10^{10}$ ,  $10^{10}$ ,  $5 \times 10^9$ . When the spring constant is on the order of  $10^{11}$ , it is assumed there is no crack between the fiber and

matrix interface. On the other hand, when the spring constants are of a very low order of magnitude, it means there is complete debonding between the fiber and matrix. Otherwise, there is a partial debonding. The results are shown in Figures 10-14 for the displacement control model. The results show that if an interface crack occurs (meaning that spring constant decreases), the composite material property of the longitudinal elastic modulus  $E_x$  will not be influenced. Both transverse elastic and shear moduli decrease as the interface crack propagates. Figures 15-19 show the solution for the force control case. In this case, the interface cracks affect the longitudinal elastic modulus and increase the transverse shear modulus, which does not make sense intuitively. As a result, the displacement control should be used for the interface crack model.



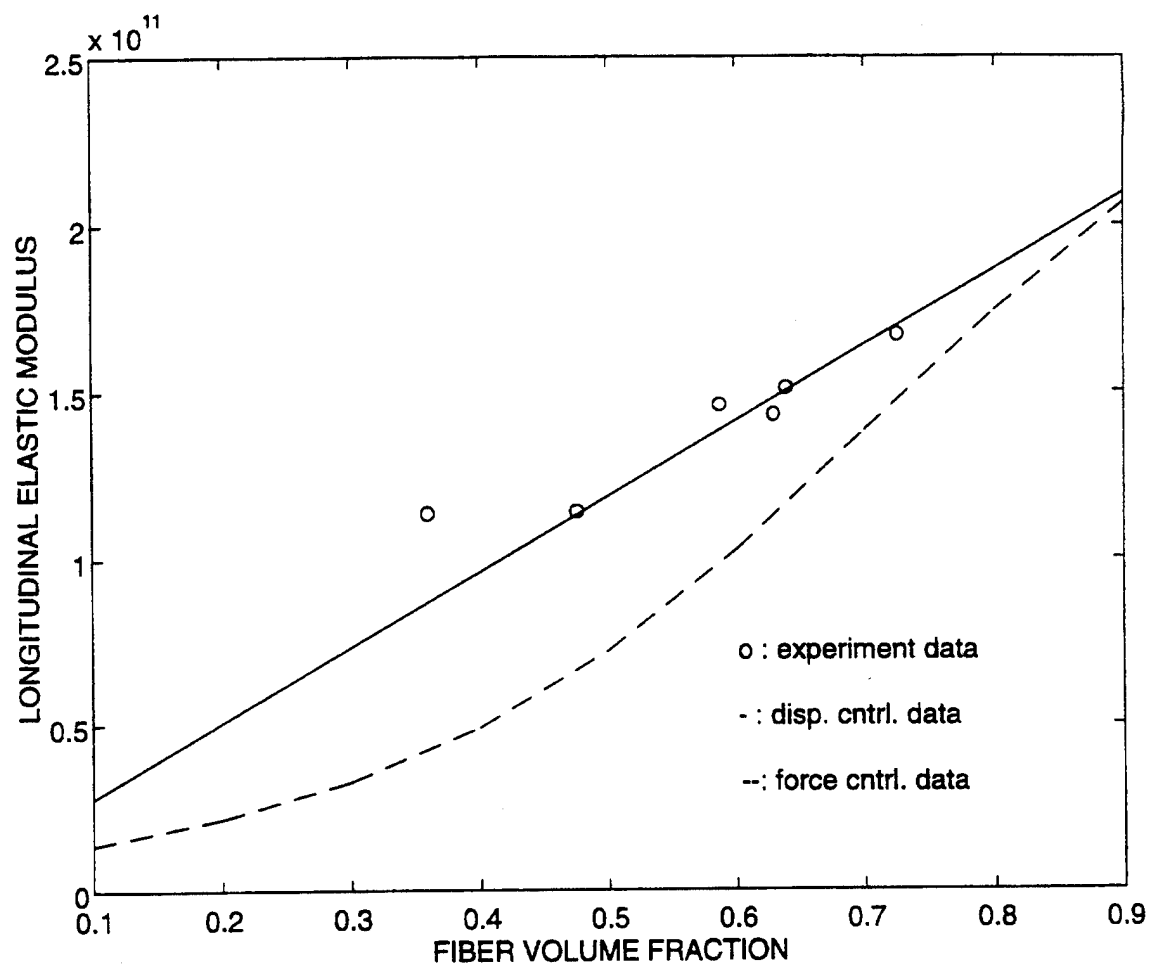


**Figure 5** Longitudinal elastic modulus of a graphite/epoxy composite

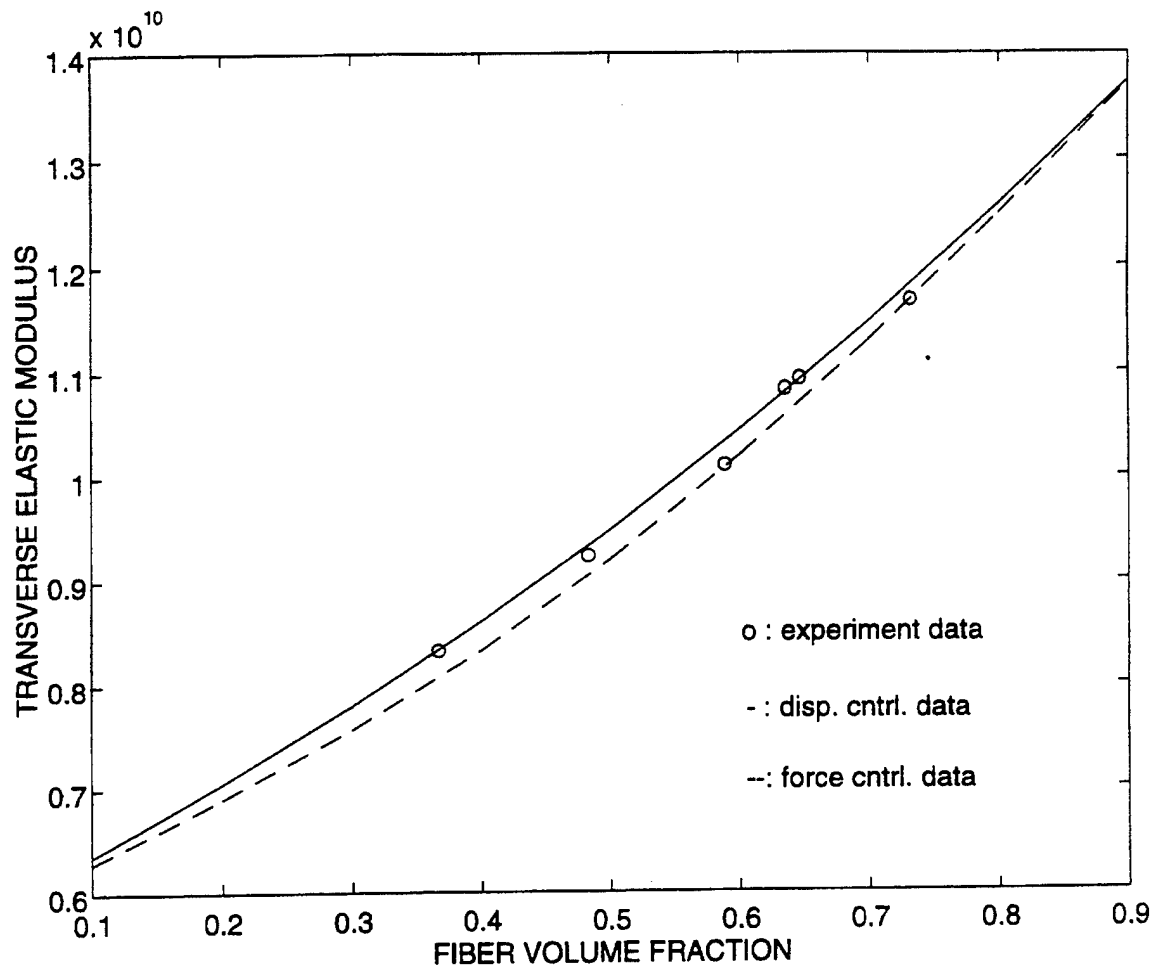


**Figure 6** Transverse elastic modulus of a graphite/epoxy composite

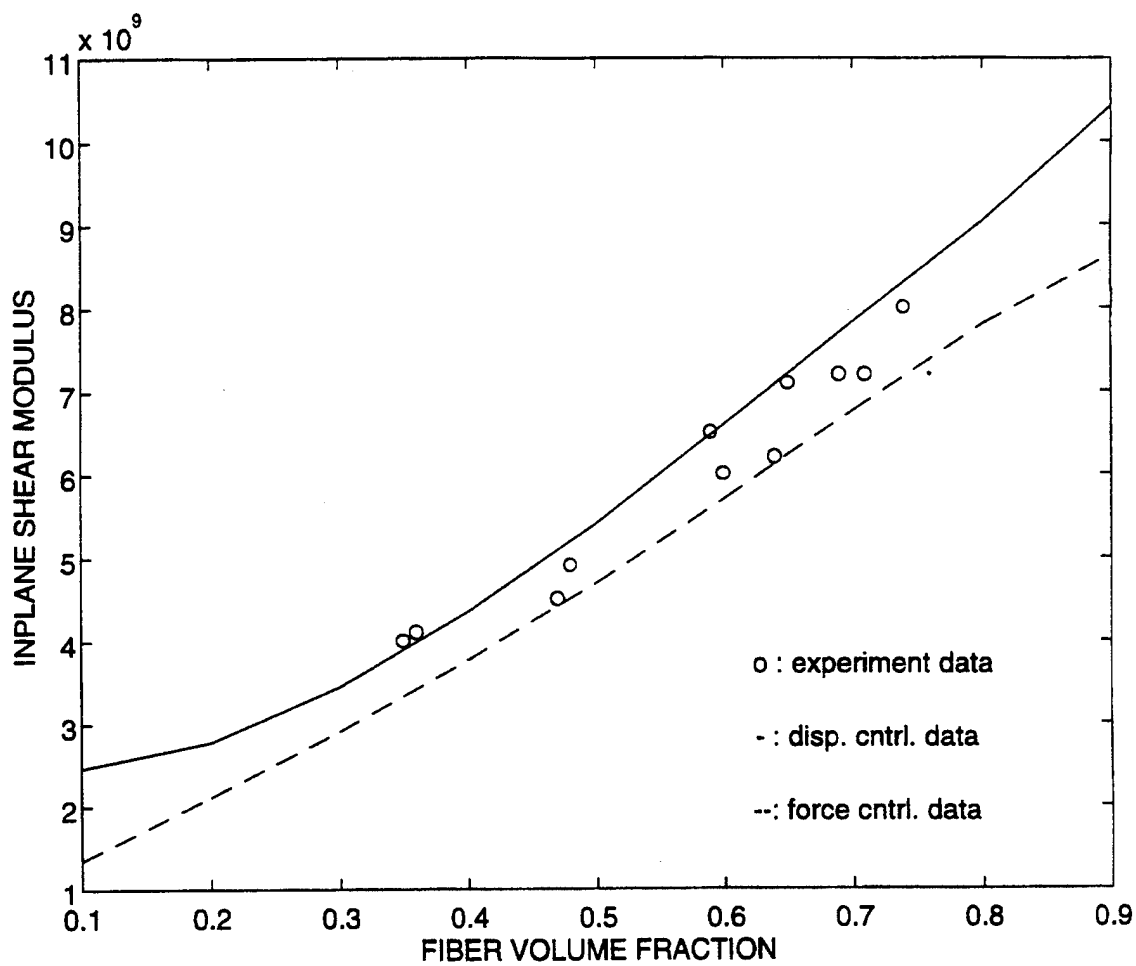


**Figure 7** Inplane shear modulus of a graphite/epoxy composite

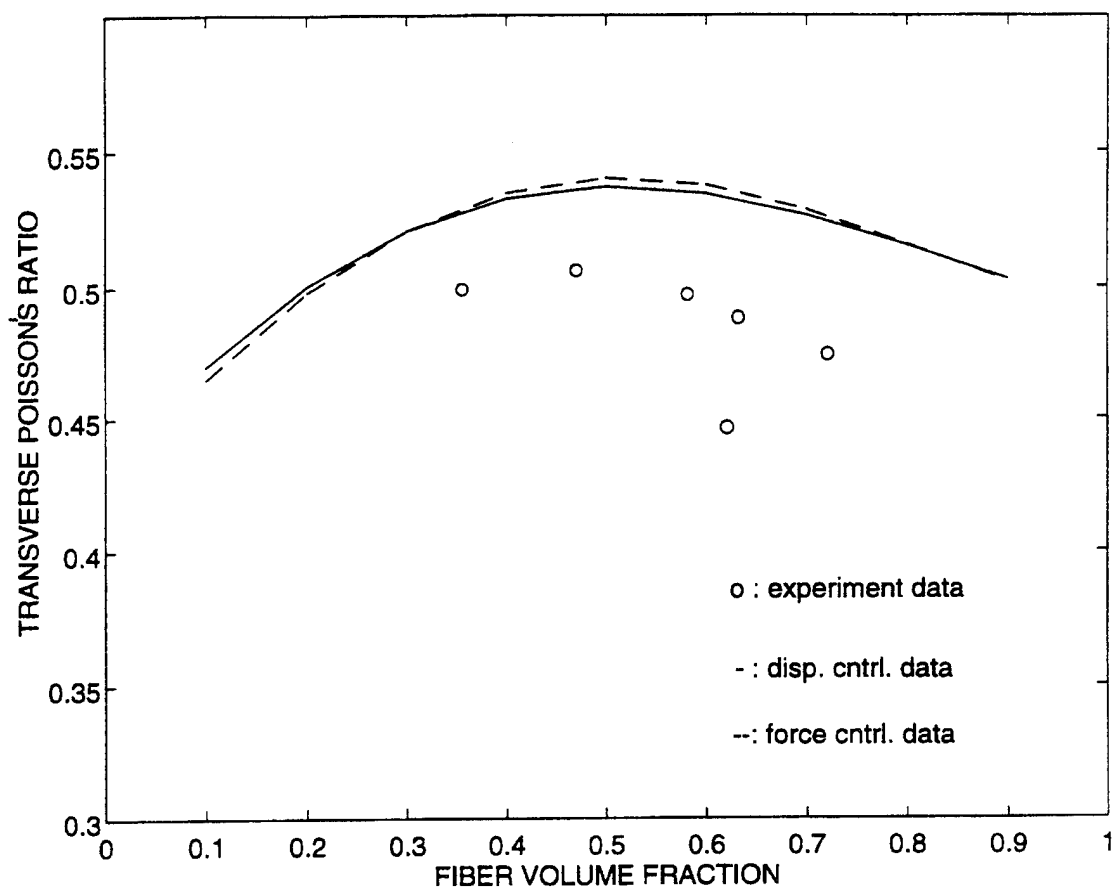


**Figure 8** Transverse Poisson's ratio of a graphite/epoxy composite

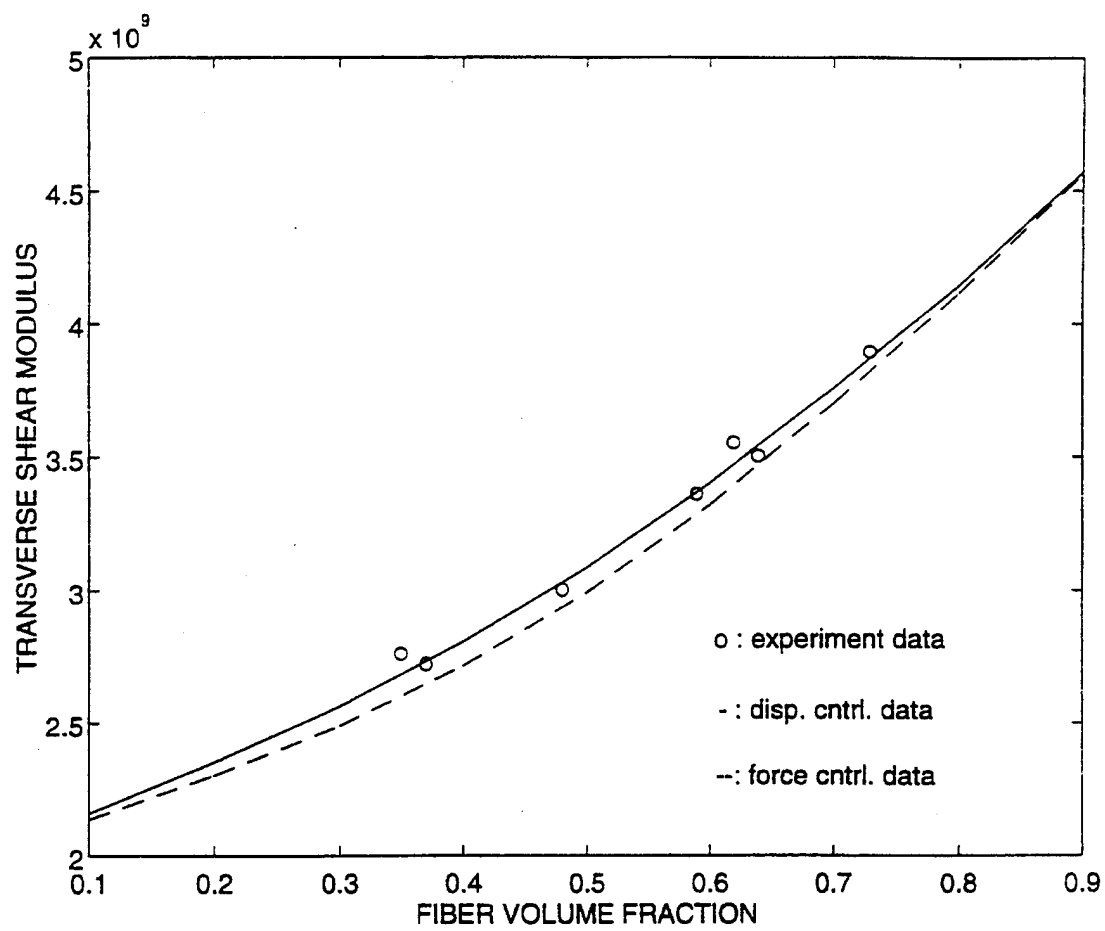


**Figure 9** Transverse shear modulus of a graphite/epoxy composite

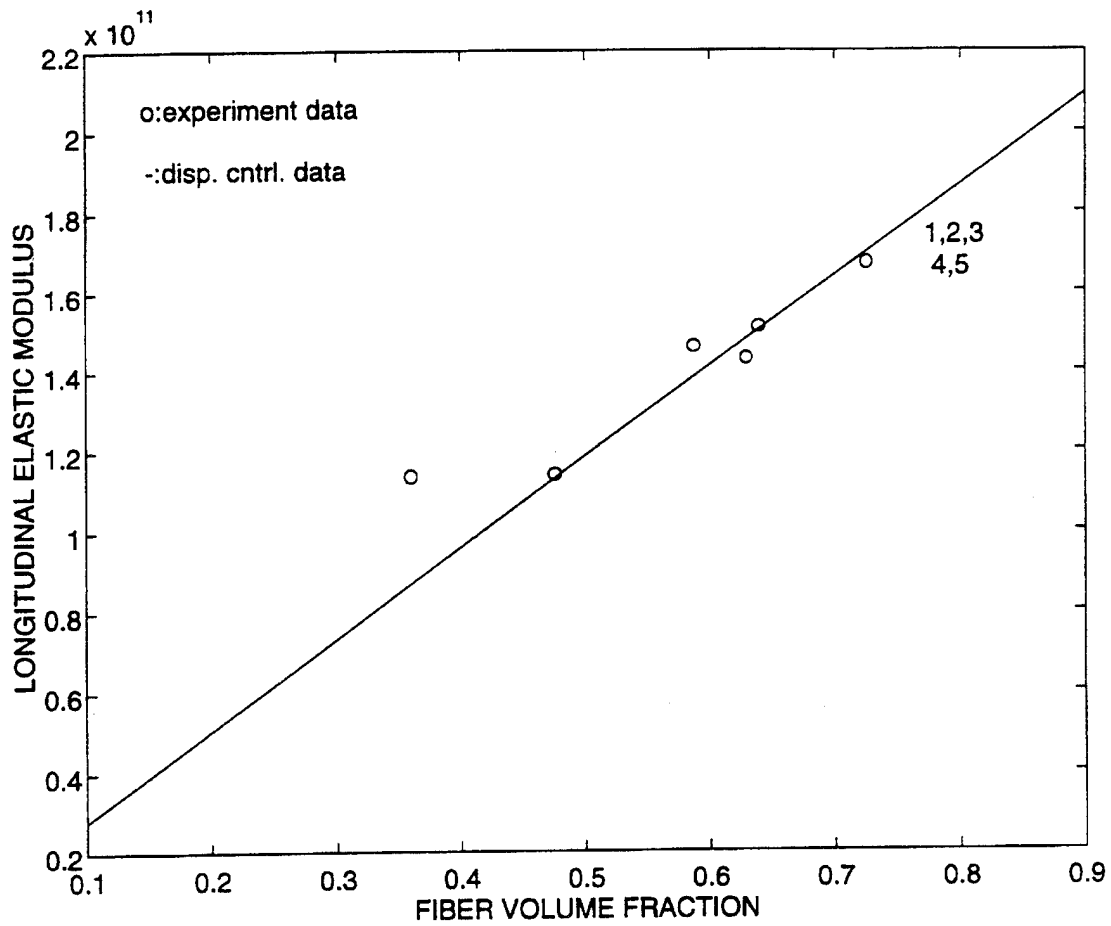


**Figure 10** Longitudinal elastic modulus of a graphite/epoxy composite with interface crack  
 (spring constant : 1  $\rightarrow 10^{11}$  2  $\rightarrow 5 \times 10^{10}$  3  $\rightarrow 2 \times 10^{10}$  4  $\rightarrow 10^{10}$  5  $\rightarrow 5 \times 10^9$ )

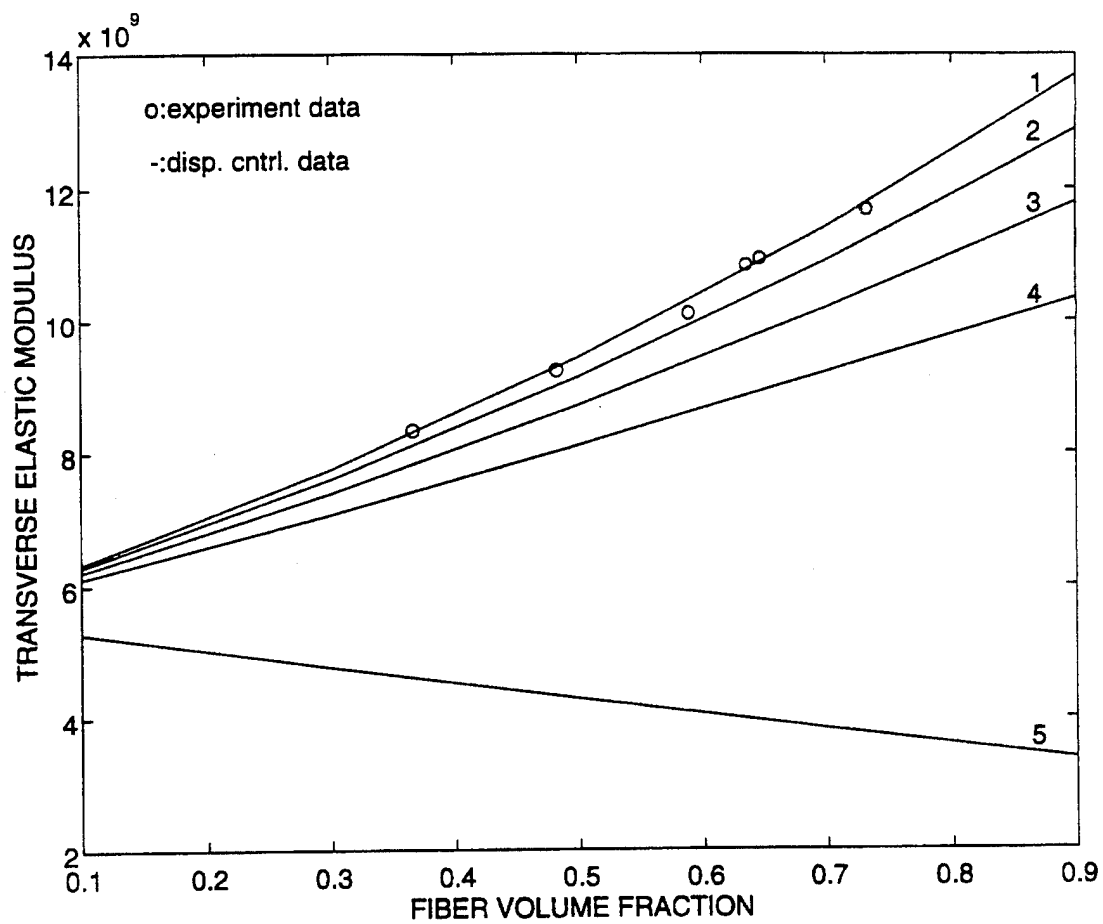


**Figure 11** Transverse elastic modulus of a graphite/epoxy composite with interface crack  
 (spring constant : 1  $\rightarrow 10^{11}$  2  $\rightarrow 5 \times 10^{10}$  3  $\rightarrow 2 \times 10^{10}$  4  $\rightarrow 10^{10}$  5  $\rightarrow 5 \times 10^9$ )

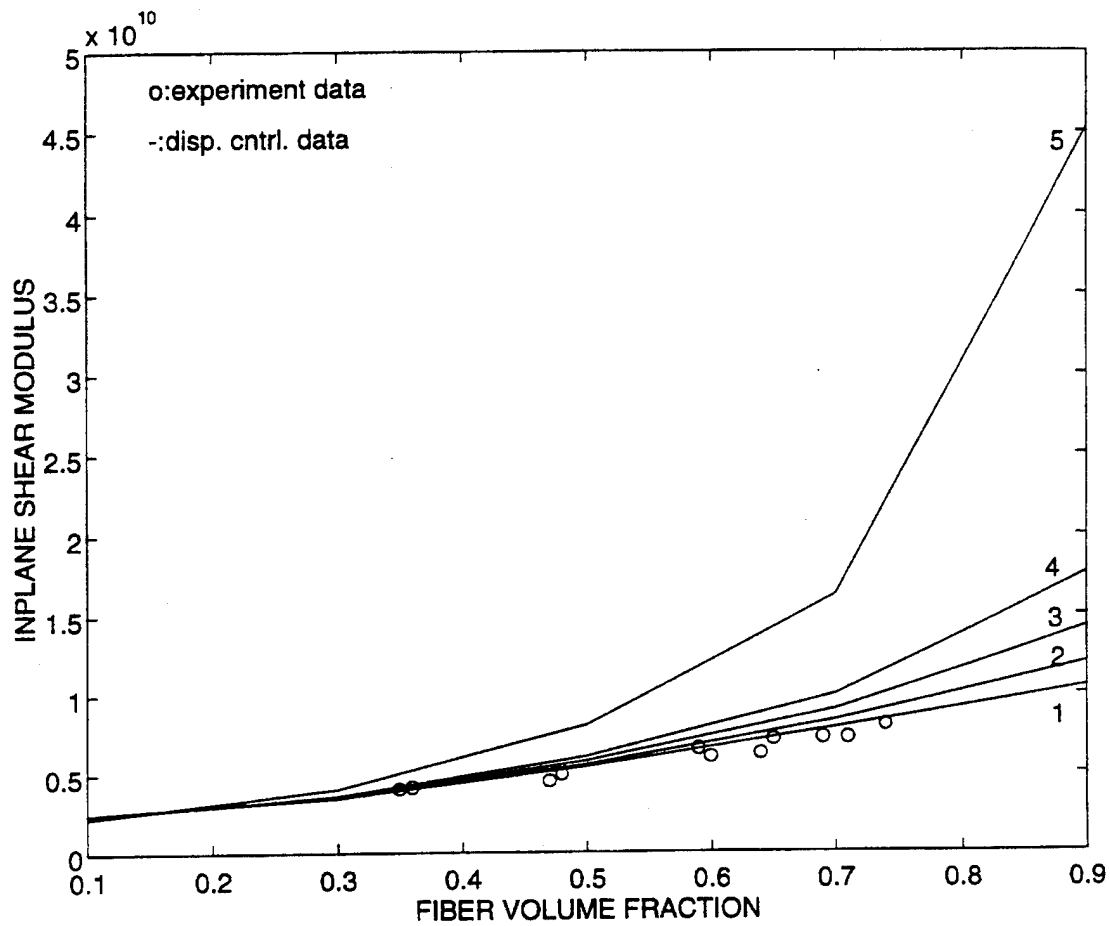


**Figure 12** Inplane shear modulus of a graphite/epoxy composite with interface crack  
 (spring constant : 1  $\rightarrow 10^{11}$  2  $\rightarrow 5 \times 10^{10}$  3  $\rightarrow 2 \times 10^{10}$  4  $\rightarrow 10^{10}$  5  $\rightarrow 5 \times 10^9$ )



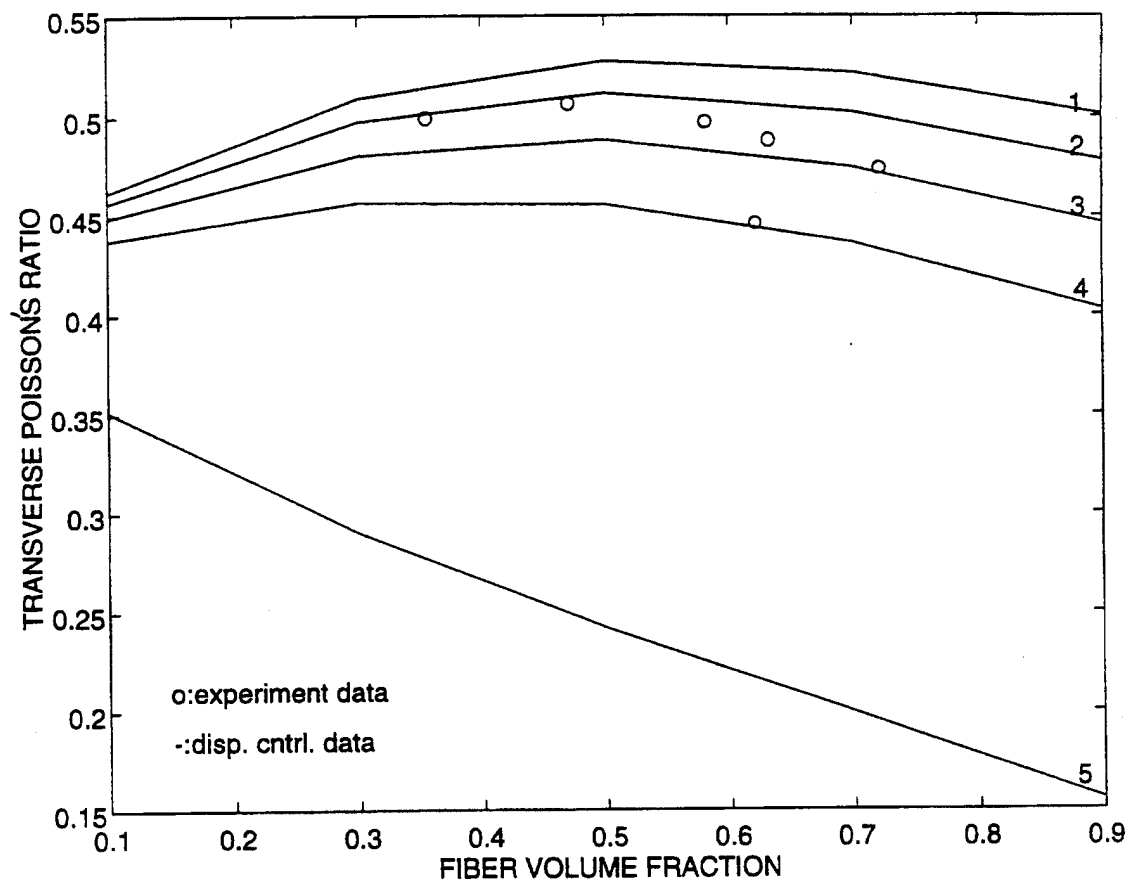


**Figure 13** Transverse Poisson's ratio of a graphite/epoxy composite with interface crack  
(spring constant : 1  $\rightarrow 10^{11}$  2  $\rightarrow 5 \times 10^{10}$  3  $\rightarrow 2 \times 10^{10}$  4  $\rightarrow 10^{10}$  5  $\rightarrow 5 \times 10^9$ )

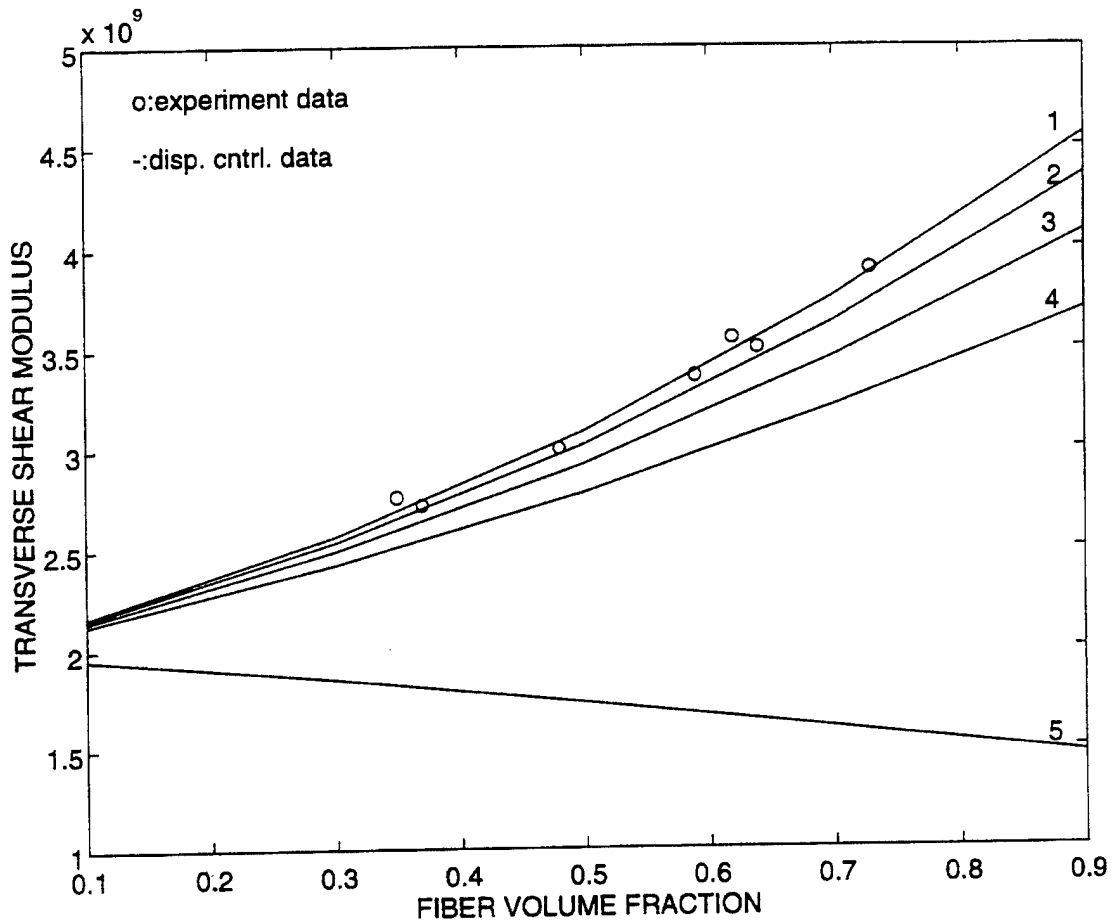


**Figure 14** Transverse shear modulus of a graphite/epoxy composite with interface crack  
 (spring constant : 1  $\rightarrow 10^{11}$  2  $\rightarrow 5 \times 10^{10}$  3  $\rightarrow 2 \times 10^{10}$  4  $\rightarrow 10^{10}$  5  $\rightarrow 5 \times 10^9$ )

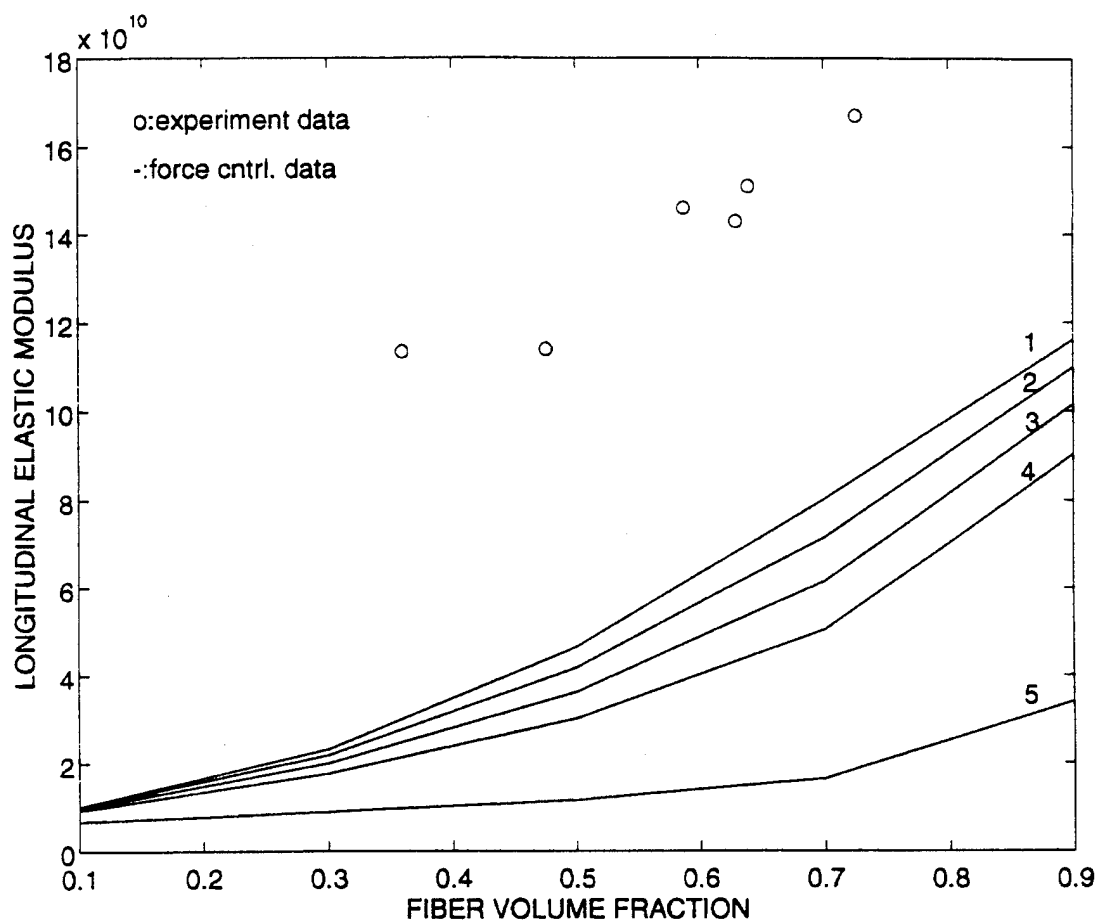


**Figure 15** Longitudinal elastic modulus of a graphite/epoxy composite with interface crack  
(spring constant : 1  $\rightarrow 10^{11}$  2  $\rightarrow 5 \times 10^{10}$  3  $\rightarrow 2 \times 10^{10}$  4  $\rightarrow 10^{10}$  5  $\rightarrow 5 \times 10^9$ )

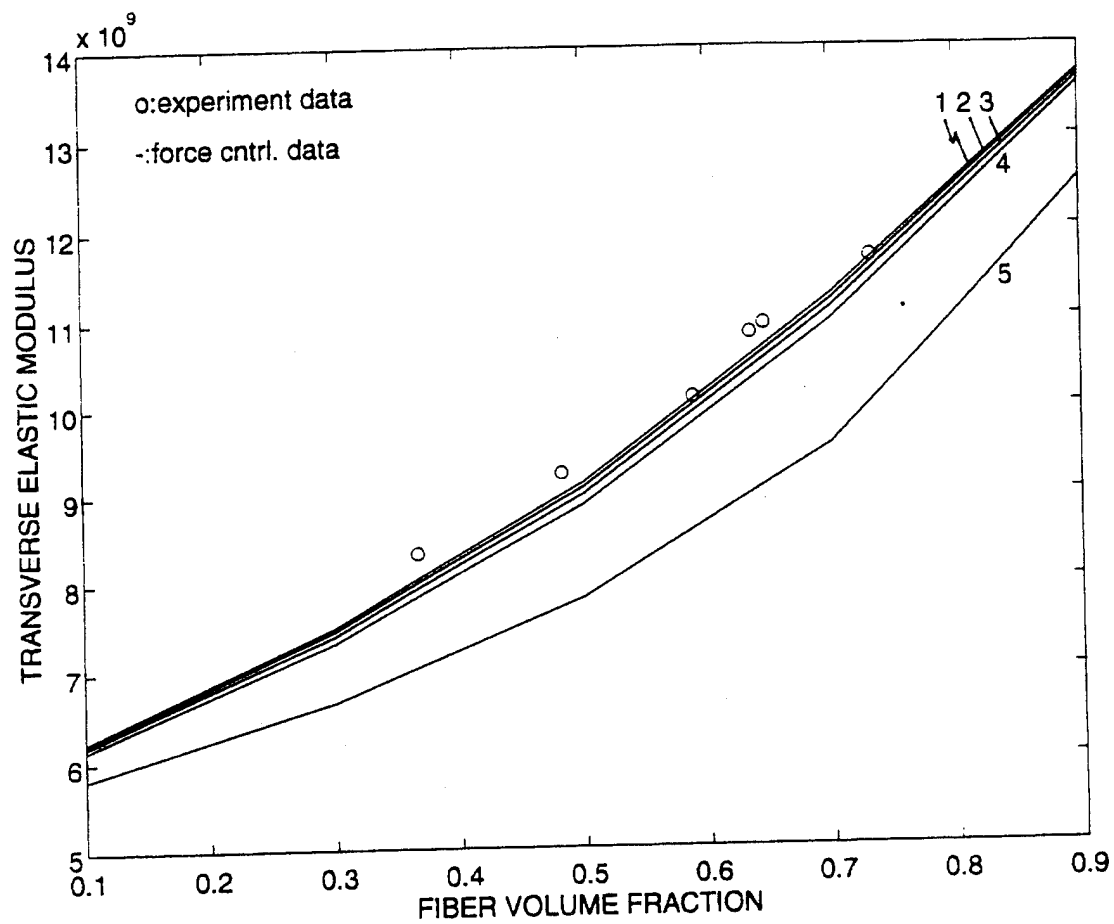


**Figure 16** Transverse elastic modulus of a graphite/epoxy composite with interface crack  
 (spring constant : 1  $\rightarrow 10^{11}$  2  $\rightarrow 5 \times 10^{10}$  3  $\rightarrow 2 \times 10^{10}$  4  $\rightarrow 10^{10}$  5  $\rightarrow 5 \times 10^9$  )

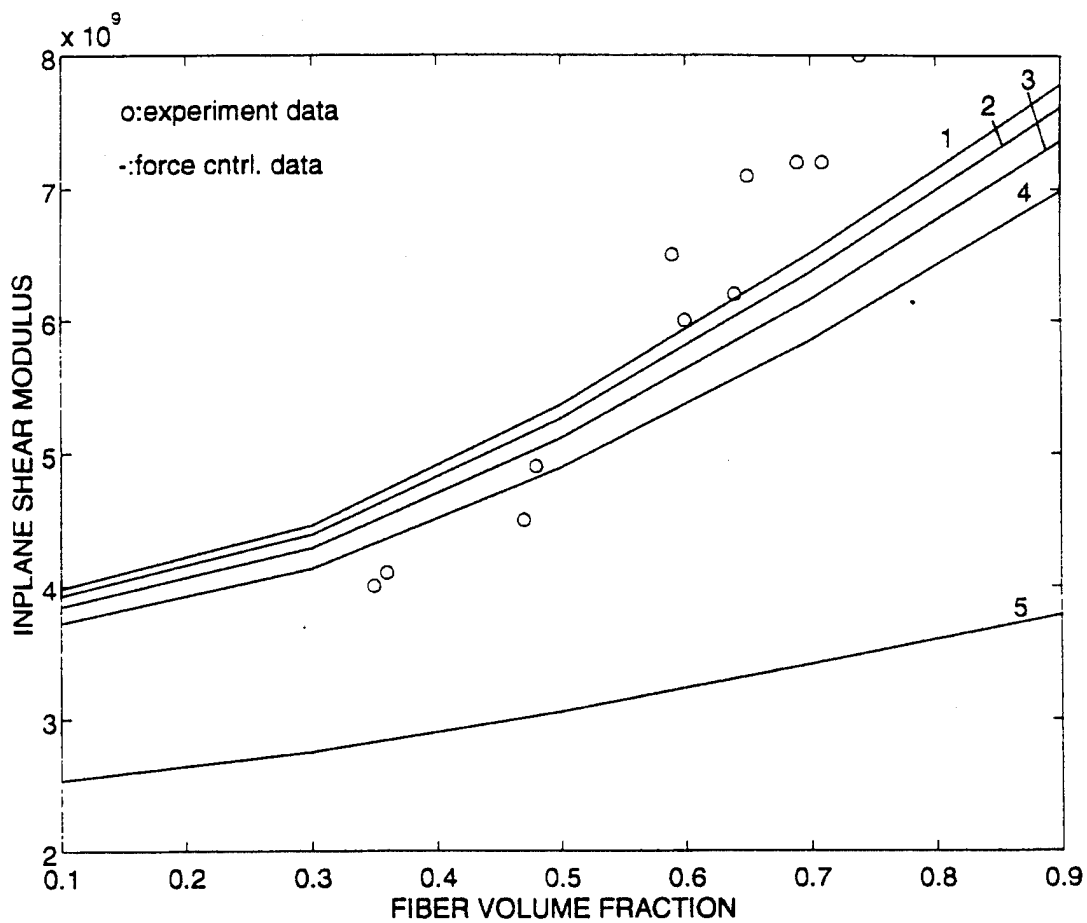


**Figure 17** Inplane shear modulus of a graphite/epoxy composite with interface crack  
 (spring constant : 1  $\rightarrow 10^{11}$  2  $\rightarrow 5 \times 10^{10}$  3  $\rightarrow 2 \times 10^{10}$  4  $\rightarrow 10^{10}$  5  $\rightarrow 5 \times 10^9$ )

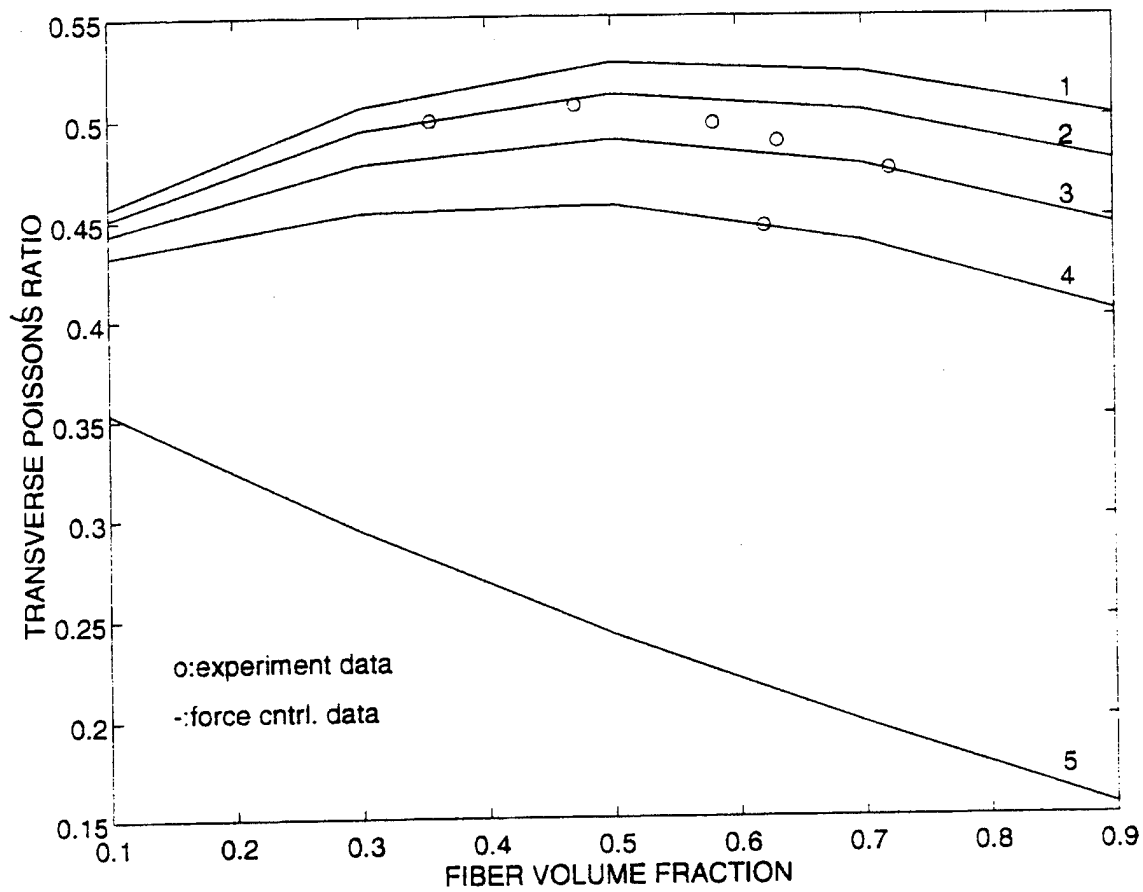


**Figure 18** Transverse Poisson's ratio of a graphite/epoxy composite with interface crack  
(spring constant : 1  $\rightarrow 10^{11}$  2  $\rightarrow 5 \times 10^{10}$  3  $\rightarrow 2 \times 10^{10}$  4  $\rightarrow 10^{10}$  5  $\rightarrow 5 \times 10^9$ )

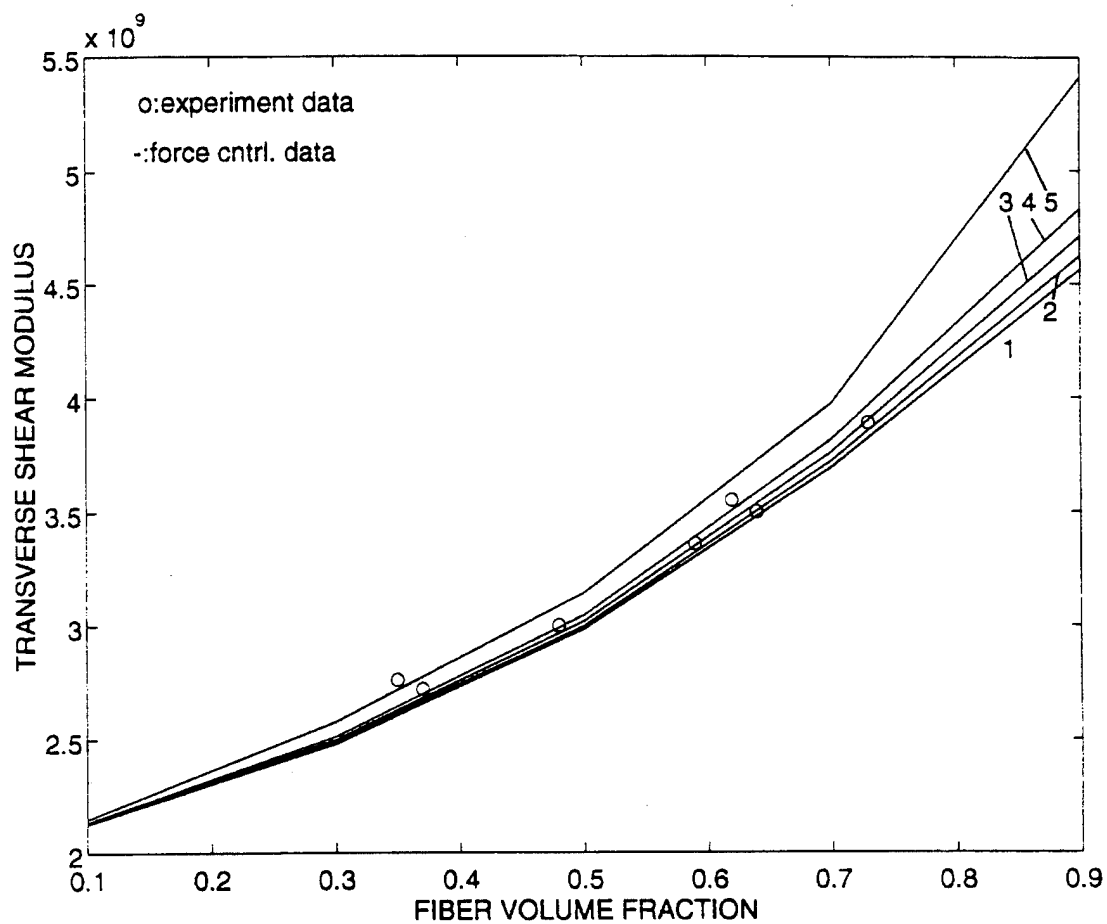


**Figure 19** Transverse shear modulus of a graphite/epoxy composite with interface crack  
(spring constant : 1  $\rightarrow 10^{11}$  2  $\rightarrow 5 \times 10^{10}$  3  $\rightarrow 2 \times 10^{10}$  4  $\rightarrow 10^{10}$  5  $\rightarrow 5 \times 10^9$  )





#### IV. CONCLUSIONS AND RECOMMENDATION

In this study, a modified analytical micro-mechanics model and 3-D FEM models were presented in order to predict the effective material properties of composites based on their constituent material properties. Then, we can summarize as follows :

1. For the analytical model, the new model was slightly better than the old models in predicting the transverse elastic modulus. Other properties were the same between the two models.
2. This research demonstrates that the 3-D FEM programmed by the MATLAB software can be efficiently used to model the behavior of fibrous composite material. Comparisons between the predicted values and experimental data proved the accuracy of the present model.
3. For fiber dominated composite materials, using displacement boundary control can provide better results than using force boundary control, especially for the longitudinal elastic modulus.
4. If there are more elements, we might obtain better results under force boundary control. However, using more elements is computationally expensive.
5. The FEM model can be expanded to analyze elastic or non-elastic behavior. We can also model interfacial cracks between the fiber and matrix. For both cracked and uncracked composites, comparisons between the present predicted values and experimental data proved the validity and accuracy of the present model.
6. For a partial interfacial debonding between the fiber and matrix, the proper spring constants may be obtained from a more detailed finite element analysis of micromechanics.



## REFERENCE LIST

1. Kwon, Y. W., "Calculation of Effective Moduli of Fibrous Composites with Micro-Mechanical Damage," Composite Structures, Vol. 25.
2. Aboudi, J., "Micromechanical Analysis of Composites by the Method of Cells," Appl. Mech. Rev., July 1989.
3. Kwon, Y. W. and J. M. Berner, "Numerical Modeling of Stiffness Reduction Due to Transverse Cracking in Unidirectional Composites," Computational Engineering, ed. by Kwak, B. M. and M. Tanaka, New York.
4. Reddy, J. N., An Introduction to the Finite Element Method, 2d Ed., McGraw-Hill, New York, 1993.
5. Bickford, W. B., A First Course in the Finite Element Method, Irwin, Boston, Massachusetts, 1990.
6. Kriz, R. D. and W. W. Stinchcomb, "Elastic Moduli of Transversely Isotropic Graphite Fibers and Their Composites," Exp. Mech., Feb 1979.



## APPENDIX A

1.  $\sigma_{22}^a = \sigma_{22}^b$
  2.  $\sigma_{22}^c = \sigma_{22}^d$
  3.  $\sigma_{33}^a = \sigma_{33}^c$
  4.  $\sigma_{22}^b = \sigma_{22}^d$
  5.  $a\epsilon_{22}^a + (1-a)\epsilon_{22}^b - a\epsilon_{22}^c - (1-a)\epsilon_{22}^d = 0$
  6.  $a\epsilon_{33}^a - a\epsilon_{33}^b + (1-a)\epsilon_{33}^c - (1-a)\epsilon_{33}^d = 0$
  7.  $\epsilon_{11}^a - \epsilon_{11}^b = 0$
  8.  $\epsilon_{11}^c - \epsilon_{11}^d = 0$
  9.  $\epsilon_{11}^b - \epsilon_{11}^c = 0$
  10.  $\bar{\epsilon}_{11} = a^2\epsilon_{11}^a + a(1-a)\epsilon_{11}^b + a(1-a)\epsilon_{11}^c + (1-a)^2\epsilon_{11}^d$
  11.  $\bar{\epsilon}_{22} = a^2\epsilon_{22}^a + a(1-a)\epsilon_{22}^b + a(1-a)\epsilon_{22}^c + (1-a)^2\epsilon_{22}^d$
  12.  $\bar{\epsilon}_{33} = a^2\epsilon_{33}^a + a(1-a)\epsilon_{33}^b + a(1-a)\epsilon_{33}^c + (1-a)^2\epsilon_{33}^d$
- \*  $a = \sqrt{V_f}$ , subscript "a, b, c, d" means subcell.



## APPENDIX B

$$[D] = \begin{bmatrix} D_{11} & D_{12} & D_{13} & 0 & 0 & 0 \\ D_{12} & D_{22} & D_{23} & 0 & 0 & 0 \\ D_{13} & D_{23} & D_{33} & 0 & 0 & 0 \\ 0 & 0 & 0 & G_{12} & 0 & 0 \\ 0 & 0 & 0 & 0 & G_{23} & 0 \\ 0 & 0 & 0 & 0 & 0 & G_{31} \end{bmatrix}$$

where

$$\nu = (1 + \nu_{23}) \left( 1 - \nu_{23} - 2\nu_{12}^2 E_2/E_1 \right)$$

$$\nu_{21} = \nu_{12} E_2/E_1, \quad \nu_{31} = \nu_{21}, \quad \nu_{13} = \nu_{31}$$

$$E_3 = E_2, \quad \nu_{32} = \nu_{23}$$

$$D_{11} = (1 - \nu_{23}^2) E_1/\nu, \quad D_{12} = \nu_{12} (1 + \nu_{23}) E_2/\nu$$

$$D_{13} = D_{12}$$

$$D_{22} = \left( 1 - \nu_{12}^2 E_2/E_1 \right) E_2/\nu$$

$$D_{23} = \left( \nu_{23} + \nu_{12}^2 E_2/E_1 \right) E_2/\nu$$

Beacuse  $G_{12}$  is given, therefore

$$G_{23} = E_2/2(1 + \nu_{32}), \quad G_{31} = G_{12}$$

- |   |   |
|---|---|
| <p>* <math>E_1</math> : longitudinal elastic modulus<br/> <math>E_2</math> : transverse elastic modulus<br/> <math>\nu_{12}</math> : longitudinal Poisson's ratio<br/> <math>\nu_{23}</math> : transverse Poisson's ratio</p> | <p><math>G_{12}</math> : longitudinal shear modulus<br/> <math>G_{23}</math> : transverse shear modulus</p> |
|---|---|





## APPENDIX C

$$\begin{Bmatrix} u \\ v \\ w \end{Bmatrix} = \begin{Bmatrix} H_1 0 0 & H_2 0 0 & H_3 0 0 & H_4 0 0 & H_5 0 0 & H_6 0 0 & H_7 0 0 & H_8 0 0 \\ 0 H_1 0 & 0 H_2 0 & 0 H_3 0 & 0 H_4 0 & 0 H_5 0 & 0 H_6 0 & 0 H_7 0 & 0 H_8 0 \\ 0 0 H_1 & 0 0 H_2 & 0 0 H_3 & 0 0 H_4 & 0 0 H_5 & 0 0 H_6 & 0 0 H_7 & 0 0 H_8 \end{Bmatrix} \begin{Bmatrix} u_1 \\ v_1 \\ w_1 \\ u_2 \\ v_2 \\ w_2 \\ u_3 \\ v_3 \\ w_3 \\ u_4 \\ v_4 \\ w_4 \\ u_5 \\ v_5 \\ w_5 \\ u_6 \\ v_6 \\ w_6 \\ u_7 \\ v_7 \\ w_7 \\ u_8 \\ v_8 \\ w_8 \end{Bmatrix}$$



## INITIAL DISTRIBUTION LIST

	No. Copies
1. Defense Technical Information Center Cameron Station Alexandria, Virginia 22304-6145	2
2. Library, Code 52 Naval Postgraduate School Monterey, California 93943-5101	2
3. Professor Y.W. Kwon, Code ME/Kw Department of Mechanical Engineering Naval Postgraduate School Monterey, CA 93943	2
4. Professor Robert M. Keolian, Code PH/Kn Department of Physics Naval Postgraduate School Monterey, CA 93943	1
5. Cheng, Chun-Chung 4F #13 ALY 250, Der-Yang Rd, Chiao-Shi, I-Lan Taiwan, Republic of China	2